

HALO LENSING OR LMC SELF LENSING?
INSIGHTS FROM THE HST CMD OF MACHO MICROLENSING SOURCE STARS

C. ALCOCK^{1,2}, R.A. ALLSMAN³, D.R. ALVES^{1,4}, T.S. AXELROD⁵, A.C. BECKER^{2,6}, D.P. BENNETT^{2,7},
K.H. COOK¹, A.J. DRAKE^{1,5}, K.C. FREEMAN⁵, M. GEHA^{1,9}, K. GRIEST⁸, M.J. LEHNER¹⁰,
S.L. MARSHALL¹, D. MINNITI^{1,11}, C.A. NELSON^{1,12}, B.A. PETERSON⁶, P. POPOWSKI¹, M.R. PRATT⁶,
P.J. QUINN¹³, C.W. STUBBS^{2,6}, W. SUTHERLAND¹⁴, A.B. TOMANEY⁶, T. VANDEHEI⁸, D. WELCH¹⁵

(The MACHO Collaboration)

Draft version May 20, 2019

ABSTRACT

The nature of Large Magellanic Cloud (LMC) microlensing is determined by the location of the microlensing source stars. If the source stars are in the LMC then LMC microlensing is predominantly halo-lensing, if the source stars are located behind the LMC, then LMC microlensing is dominated by self-lensing. We attempt to distinguish between source stars drawn from the average population of the LMC and source stars drawn from a population behind the LMC by examining the HST color-magnitude diagram (CMD) of microlensing source stars. We present WFPC2 HST photometry of eight MACHO microlensing source stars and the surrounding fields in the LMC. The microlensing source stars are identified by deriving accurate centroids in the ground-based MACHO images using difference image analysis (DIA) and then transforming the DIA coordinates to the HST frame. We consider in detail a model for the background population of source stars based on that presented by Zhao, Graff & Guhathakurta. In this model, the source stars have an additional reddening $\langle E(B-V) \rangle = 0.13$ mag and a slightly larger distance modulus $\langle \Delta\mu \rangle \sim 0.3$ mag than the average LMC population. We also investigate a series of source star models, varying the relative fraction of source stars drawn from the average and background populations and the displacement of the background population from the LMC. The data suggest that all of the MACHO microlensing source stars are not drawn from a background population.

1

Lawrence Livermore National Laboratory, Livermore, CA 94550
Email: alcock, kcook, adrake, cnelson, popowski, stuart@igpp.ucllnl.org

2

Center for Particle Astrophysics, University of California, Berkeley, CA 94720

3

Supercomputing Facility, Australian National University, Canberra, ACT 0200, Australia
Email: Robyn.Allsman@anu.edu.au

4

Space Telescope Science Institute, 3700 San Martin Dr., Baltimore, MD 21218
Email: alves@stsci.edu

5

Research School of Astronomy and Astrophysics, Canberra, Weston Creek, ACT 2611, Australia
Email: tsa, kcf, peterson@mso.anu.edu.au

6

Departments of Astronomy and Physics, University of Washington, Seattle, WA 98195
Email: becker, stubbs@astro.washington.edu

7

Department of Physics, University of Notre Dame, IN 46556
Email: bennett@bustard.phys.nd.edu

8

Department of Physics, University of California, San Diego, CA 92039
Email: kgriest@ucsd.edu, vandehei@astrophys.ucsd.edu

9

Department of Astronomy and Astrophysics, University of California, Santa Cruz 95064
Email: mgeha@ucolick.org

10

Department of Physics, University of Sheffield, Sheffield S3 7RH, UK
Email: m.lehner@sheffield.ac.uk

11

Depto. de Astronomia, P. Universidad Catolica, Casilla 104, Santiago 22, Chile
Email: dante@astro.puc.cl

12

Department of Physics, University of California, Berkeley, CA 94720

13

European Southern Observatory, Karl Schwarzschild Str. 2, D-8574 8 Garching bei München, Germany
Email: pjq@eso.org

14

Department of Physics, University of Oxford, Oxford OX1 3RH, U.K.
Email: w.sutherland@physics.ox.ac.uk

15

McMaster University, Hamilton, Ontario Canada L8S 4M1
Email: welch@physics.mcmaster.ca

arXiv:astro-ph/0008282v1 17 Aug 2000

1. INTRODUCTION

The single observable in microlensing studies, the event duration, admits degeneracy in the three fundamental microlensing parameters: the mass, distance and velocity of the lens. This makes it difficult to distinguish between the two main models of the Large Magellanic Cloud (LMC) microlensing: a) lenses in the halo of the Milky Way, and b) lenses in disk of the LMC. This topic has been explored extensively and attempts to distinguish between these two models have taken one of two forms: determinations based solely on the total quantity of LMC microlensing (optical depth) and determinations based on the properties of LMC microlensing events.

Early efforts focused mainly on determinations based on the microlensing optical depth. Sahu (1994) and Wu (1994) suggested that LMC self-lensing with a standard LMC geometry could reproduce the observed optical depth. This claim has since been disputed by several groups e.g., (Gould 1995; Alcock et al. 2000a) However, LMC self-lensing becomes a much more probable hypothesis if the LMC possesses a halo similar to that of the Milky Way (MW). The problem with an LMC halo is that no tracers of old populations in the LMC have ever revealed a population with high enough velocity dispersions to suggest a spheroidal component (Olszewski, Suntzeff & Mateo 1996). Recently however, N-body simulations by Weinberg (2000) suggested that the LMC's dynamical interaction with the MW may torque the LMC disk in such a way that the LMC disk is thickened and a spheroidal component is populated without isotropizing the stellar orbits and thereby leaving disklike kinematics intact. This has lent new credence to the hypothesis that LMC self-lensing can quantitatively explain observed microlensing (Weinberg 2000; Evans & Kerins 2000). These new studies have in turn been disputed by Gyuk, Dalal, & Griest (2000) who along with Alves & Nelson (2000) conclude that self-lensing models for the LMC using reasonable LMC geometries and properly field-weighted optical depths still fall well short of explaining the observed optical depth.

Recently, several groups have undertaken to distinguish between halo and self-lensing by examining the properties of microlensing events instead of (or in addition to) the total optical depth. The analysis of a few binary lens caustic crossing events is one way to resolve the LMC lensing controversy. When the caustic crossing is well resolved and the properties of the source star are well known, the distance to the lens may be determined. Thus far only one such event has occurred in the LMC (Bennett et al. 1996). The degeneracy may also be broken in certain binary source events where the lightcurve exhibits deviations from the standard microlensing fit due to the "xallarap" effect. This effect is the inverse of the parallax effect due to the motion of the Earth around the Sun, in this case the orbital motion occurs at the lensed source (Gould 1992; Alcock et al. 1995). Other methods focus on the available properties of all microlensing events. Gyuk, Dalal, & Griest (2000) and Evans & Kerins (2000) both propose methods for distinguishing between halo and self-lensing based on the geometrical distribution of source stars across the LMC. In this work we explore the suggestion of Zhao (1999), Zhao (2000), and Zhao, Graff & Guhathakurta (2000) that one may determine the location of the source stars by determining their reddening.

The available self-lensing geometries are strongly con-

strained by knowledge of the size, structure and content of the LMC (Gyuk, Dalal, & Griest 2000) and the only potentially viable model remaining for a self-lensing population large enough to explain the observed optical depth is a thick three dimensional structure behind the LMC. Since this structure lies behind the LMC it should suffer from the internal extinction of the LMC. In addition, this structure may be displaced from the LMC by some amount, a feature which would manifest itself with a larger distance modulus. Zhao, Graff & Guhathakurta (2000) present a preferred model for this background population with an additional mean reddening relative to the average population of the LMC $\langle E(B-V) \rangle = 0.13$ mag and a displacement from the LMC of ~ 7.5 kpc resulting in an increase of distance modulus of $\langle \Delta\mu \rangle \sim 0.3$ mag. If the source stars are drawn from this background population, then LMC microlensing is dominated by self-lensing events. Conversely, if the source stars are drawn from the average population of the LMC, then LMC microlensing is dominated by halo-lensing events.

We compare the likelihood of the predominantly halo-lensing model (Model 1) to the predominantly self-lensing model (Model 2) by comparing an Hubble Space Telescope (HST) CMD of MACHO microlensing source stars to efficiency weighted CMDs of the average population of the LMC and the Zhao, Graff & Guhathakurta (2000) background population. In §2 we construct a CMD of the average LMC population by combining the CMDs of eight HST Wide Field Planetary Camera 2 (WFPC2) fields centered on past MACHO microlensing events in the outer LMC bar. In §3 we describe the identification of the microlensing source stars in these fields by difference image analysis (DIA). In §4 we construct the background population CMD by shifting the HST CMD by the appropriate amount of extinction and distance modulus. We then describe the convolution of the average and background HST CMDs with the MACHO efficiency for detecting a microlensing event in a source star of given magnitude. In §5 we determine the likelihoods that the microlensing source stars were drawn from the average population of the LMC (Model 1) or from a population of background source stars (Model 2) by using Kolmogorov-Smirnov (KS) tests to compare our observed and model distributions. Finally, in §6 we generalize our analysis and consider models that are both less and more extreme than Model 2.

2. HST OBSERVATIONS

Observations were made with the WFPC2 on HST between May 1997 and October 1999 through the F555W (*V*) and F814W (*I*) filters. The Planetary Camera (PC) was centered on the location of past MACHO microlensing events. The microlensing events, positions, and exposure times are listed in Table 1.

Multiple exposures of a field were combined using a sigma-clipping algorithm to remove deviant pixels, usually cosmic rays. The PC has a pixel size of $0.046''$ which easily resolves the great majority of stars in our frames. Most stars are also resolved in the Wide Field (WF) fields which have a pixel size of $0.1''$. Instrumental magnitudes were calculated from aperture photometry using DAOPHOT II (Stetson 1987, 1991) with a radius of $0.25''$ and centroids derived from point-spread fitting photometry. Aperture corrections to $0.5''$ were performed

individually for each frame by finding the median aperture correction for the 50 brightest stars in each field. We correct for the WFPC2 charge transfer effect using the equations from Instrument Science Report WFPC2 97-08. We also make the minimal corrections for contaminants which adhere to the cold CCD window according to the WFPC2 Instrument Handbook. We transform our instrumental magnitudes to Landolt V and I using the calibrations from Holtzman et al. (1995).

We create a composite LMC CMD by combining the PC and WF photometry for all of our fields except the field of LMC-1. In the case of LMC-1 the V and I observations were taken at different roll angles and there is little area of overlap except in the PC frame. We therefore include the PC field from LMC-1 but not the WF fields. The composite HST CMD is shown in Figure 1.

3. SOURCE STAR IDENTIFICATION THROUGH DIFFERENCE IMAGE ANALYSIS

A ground-based MACHO image has a pixel size of $0.6''$ and a seeing of at least $1.0-1.5''$. Thus, in a typically crowded region of the outer LMC bar, a MACHO seeing disk will contain 3-5 stars of $V \lesssim 24$. This means that “stars” in ground-based MACHO photometry are usually not single stars at all, but rather blended composite objects made up of several fainter stars. Henceforth, we distinguish between these two words carefully, using *object* to denote a collection of stars blended into one seeing disk, and *star* to denote a single star, resolved in an HST image or through DIA. The characteristics of the MACHO object that was lensed tell us little about the actual lensed star. However, with the microlensing object centroid from the MACHO images we can hope to identify the microlensing source star in the corresponding HST frame.

A direct coordinate transformation from the MACHO frame to the HST frame often places the baseline MACHO object centroid in the middle of a cluster of faint HST stars with a single star clearly identified. To resolve this ambiguity we have used DIA. This technique is described in detail in Tomaney & Crots (1996), but we review the main points here. DIA is an image subtraction technique designed to provide accurate photometry and centroids of variable stars in crowded fields. The basic idea is to subtract from each program image a high signal-to-noise reference image, leaving a differenced image containing only the variable components. Applied to microlensing, we subtract baseline images from images taken at the peak of the microlensing light curve, leaving a differenced image containing only the flux from the microlensing source star and not the rest of the object. We also find a centroid shift between the baseline image and the differenced image towards the single star that was microlensed. If the centroid from the differenced image is transformed to the HST frame we find that it usually clearly identifies the HST microlensed source star. This process is illustrated in Figures 2 and 3.

This technique allows us to unambiguously identify 7 of 8 microlensed source stars. In the case of LMC-9 the DIA centroid lands perfectly between two stars; fortunately these two stars are virtually identical sub-giants and the choice between the two has no effect on our results. Our identification of LMC-5 revealed it to be the rather rare case of a blended HST star. Although the DIA centroid clearly identified only one star of the pair, at an aperture of $0.25''$ the flux of the source star was contaminated by that of its neighbour. In this case we first subtracted the neighbouring star and then performed aperture

photometry as described in §2. In Table 2 we present the V magnitudes and $(V-I)$ colors of our source stars. The errors presented here are the formal photon counting errors returned by DAOPHOT II. We estimate that all WFPC2 magnitudes have an additional $0.02-0.03$ mag uncertainty due to aperture corrections. In the case of LMC-9 we tabulate both possibilities and use LMC-9a in the remainder of this work.

4. CREATION OF THE MODEL SOURCE STAR POPULATIONS

If the microlensing events are due to halo lenses then one would expect the distribution of observed microlensing source stars to be randomly drawn from the average population of the LMC corrected only for the MACHO detection efficiency for stars of a given magnitude (Model 1). We assume that the population of the LMC is well represented by our composite HST CMD to $V \lesssim 24$. If the microlensing events are self-lensing events we expect the source stars to be drawn from a background population which suffers from the internal extinction of the LMC (Model 2). To represent such a background population we shift the composite HST CMD according to the amounts suggested by Zhao, Graff & Guhathakurta (2000), $\langle E(B-V) \rangle = 0.13$ and $\Delta\mu = 0.3$. Since, Holtzman et al. (1995) calibrate instrumental WFPC2 magnitudes to the Landolt system, we use the appropriate Landolt system extinction coefficients of Table 6 in Schlegel, Finkbeiner & Davis (1998) to translate these estimates to our filters. The total shifts, taking into account both reddening and distance modulus, are

$$\Delta V = A_V + \Delta\mu = 0.73, \quad \Delta(V-I) = E(V-I) = 0.18 \quad (\text{Model 2})$$

Thus far we have constructed two CMDs representing the distribution of all possible source stars down to $V \sim 24$. However, not all possible microlensing events are detected in the MACHO images. To create a CMD representing a population of source stars which produce detectable microlensing events we must convolve the HST CMD with the MACHO detection efficiency. The MACHO efficiency pipeline is extensively described in Alcock et al. (2000a) and Alcock et al. (2000b) and the detection efficiency as a function of stellar magnitude, V_{star} , and Einstein ring crossing time has been calculated. We average this function over the event durations of the candidate microlensing events derived using criterion A from Alcock et al. (2000a) and present the MACHO detection efficiency as a function of V_{star} in Figure 4. We convolve this function with our HST CMDs to produce the final Models 1 and 2 distributions of source stars. In Figure 5, we show our model source star populations with the observed microlensing source stars of Table 2 overlaid as large red dots.

This procedure admits several assumptions. First, we assume that our eight HST fields collectively well represent the stellar population of the LMC disk. This assumption has two parts, the first being that an observation at a random line of sight in the LMC bar is dominated by stars in the LMC disk and the second that the stellar population across the LMC is fairly constant. The first part holds so long as the surface density of the background population is much smaller than that of the LMC itself. If this were not the case, this population would have been directly detected. The second part has been confirmed by many LMC population studies including Alcock et al. (2000b), Olsen (1999), and Geha et al. (1998), as well as our own comparison of individual CMDs and luminosity functions. Second, we assume that the underlying stellar content of the background population is identical to that of the LMC.

5. HALO LENSING OR SELF LENSING?

We now ask the question whether the CMD of microlensed source stars is consistent with the average population of the LMC (Model 1) or whether it is more consistent with a background population (Model 2). Examining Figure 5, while referring to Table 2, we see that Model 2 moves the event just below the clump, LMC-1, into the clump, a much denser and thus more probable region of the CMD. However, Model 2 also displaces the events on the sub-giant branch, LMC-5 and LMC-9, from the sub-giant branch and nearly removes our brightest main sequence event, LMC-14, from the upper main-sequence. The trade off between these effects makes Model 1 appear to be the more likely. To quantify this impression we perform a two-dimensional Kolmogorov-Smirnov (KS) test.

In the familiar one dimensional case, a KS test of two samples with number of points N_1 and N_2 returns a distance statistic D , defined to be the maximum distance between the cumulative probability functions at any ordinate. Associated with D is a corresponding probability $P(D)$ that if two random samples of size N_1 and N_2 are drawn from the same distribution a worse value of D will result. This is equivalent to saying that we can exclude the hypothesis that the two samples are drawn from the same distribution at confidence level of $1.0 - P(D)$. If $N_2 \gg N_1$ then this is also equivalent to excluding at a $1.0 - P(D)$ confidence level the hypothesis that sample 1 is drawn from sample 2.

The concept of a cumulative distribution is not defined in more than one dimension. However, it has been shown that a good substitute in two dimensions is the integrated probability in each of four right-angled quadrants surrounding a given point (Fasano & Franceschini 1987; Peacock 1983). Leaving aside the exact algorithmic definition (Press et al. 1992) a two-dimensional KS test yields a distance statistic D and a corresponding $P(D)$ with the same interpretation as in the one dimensional case.

We use the two dimensional KS test to test hypothesis that the CMD of observed MACHO microlensing events is drawn from the same population as each of the model source star distributions. We find distance statistics $D_1 = 0.390 \pm 0.006$ and $D_2 = 0.456 \pm 0.008$, for Models 1 and 2 respectively. Each of these distance statistics has a corresponding probability, $P(D)$, that if we draw an 8 star samples from the model population a larger value than D will result. As explained above, this is equivalent to excluding this model population as the actual parent of our observed microlensing source stars at a confidence level of $1.0 - P(D)$. These probabilities are $P_1 = 0.343 \pm 0.032$ and $P_2 = 0.138 \pm 0.021$. The error quoted for each of these quantities is the scatter about the mean value in 100 simulations for each model. Because the creation of the efficiency convolved CMD is a weighted random draw from the HST CMD, the model population created in each simulation differs slightly. This in turn leads to small differences in the KS statistics.

These results tell us that these 8 MACHO events are insufficient to reliably distinguish the halo and self lensing hypothesis. The best we can do is to exclude Model 2 at the statistically marginal 86% confidence level. While we cannot gain any new information by projecting our two dimensional data set onto the V -magnitude and $(V - I)$ -color axes, we can hope to gain some insight into the competing factors which lead to such similar results for both models in the two dimensional KS tests.

In Figure 6 we present the color distributions of the observed microlensing source stars by dashed lines, and those of the

model efficiency convolved CMD as solid lines. In Figure 7 we show the corresponding luminosity distributions. All curves have been normalized to have the same total area. We show the actual number of stars represented by the dashed lines on the right hand scale and the actual number of stars represented by the solid lines on the left hand side. We test whether or not the observed MACHO microlensing source stars were drawn from each of the model distributions using 1-D KS tests. The reader is cautioned that while we will discuss the relative shape of these binned histograms in the following paragraphs to illustrate key features of our models, one dimensional KS tests are not dependent on binning (which is a highly subjective procedure). We also note that while the Poisson noise is negligible for the solid curves, it is quite high for the dashed curves.

First, we consider the color distributions. We note Model 2 results in color distributions which decreases significantly in the region $0.2 \lesssim (V - I) \lesssim 1.0$. This noticeable change in shape from our Model 1 distribution occurs because of the relative location of the first slice in color which intersects the lower main sequence (LMS). For instance, in Model 1 this slice occurs at $(V - I) \sim 0.6$ and $\langle V \rangle \sim 22$. In Model 2, the shift in color and magnitude means that the first slice in color does not intersect the LMS until $(V - I) \sim 0.80$ and $\langle V \rangle \sim 23$. In Model 1 the slices in color intersect the LMS before the MACHO detection efficiency has fallen to zero and we include many stars from below the turnoff in the color distribution, keeping the color distributions relatively constant until we reach the giant branch at $(V - I) \sim 1.0$. By $V \sim 23$ the MACHO efficiency has fallen to zero and so in Model 2 the efficiency convolution removes the LMS, leaving very few stars in the region $0.2 \lesssim (V - I) \lesssim 1.0$. The color distributions of observed MACHO microlensing suggests a very flat distribution, which seems more consistent with the shape of the Model 1 distribution. 1-D KS tests confirm this suspicion yielding probabilities $P_1(V - I) = 0.927 \pm 0.017$ and $P_2(V - I) = 0.065 \pm 0.010$ for Models 1 and 2 respectively. Therefore, the color distributions alone strongly favor Model 1.

Next, we consider the luminosity distributions. For our Model 1 source star population find a probability that the observed microlensing events are drawn from this luminosity distribution of $P_1(V) = 0.113 \pm 0.010$. Model 2 increases this probability, giving $P_2(V) = 0.230 \pm 0.021$. The errors quoted are the standard deviation about the mean value for a hundred simulations.

The luminosity distributions suggest that both models are marginal and favor Model 2. This result reflects two gross features of the observed source star distribution: there are not enough microlensing source stars in the clump and there are too many microlensing source stars at $V \lesssim 21$. In Model 1 we see the effect of the giant branch clump in the maximum of the model luminosity distribution in the $19.0 < V < 19.5$ bin. While the peak in the luminosity distribution is due to the clump, we note that stars in this magnitude bin from the UMS are also included. There is no corresponding peak in the observed microlensing event distribution. In Model 2 the maximum in the model luminosity distributions is shifted to the $19.5 < V < 20.0$ bin, centering the maximum on our one clump event, LMC-1. However, this does nothing to resolve the disparity between the number of expected and detected events in the maximum as the number of expected peak events also changes. In Model 1 we expect 2 events in the peak of the distribution and find 1 (which actually comes from the UMS), while in Model 2 we expect 2.3 events in the peak and find 1. The

number of expected peak events in Model 2 is higher because, as discussed above, the efficiency convolution in this model removes more faint stars, making the clump all the more important. Thus, the higher likelihood of Model 2 is not driven by clump events, but rather by upper main sequence events LMC-6 and LMC-8 which are shifted towards the maximum in the expected distribution.

The overall low likelihood of both models is largely driven by the overabundance of faint microlensing events. This may reflect a problem with the MACHO efficiencies, or may simply be a result of small number statistics. This overabundance amounts to only an “extra” 1-2 faint source star events.

Our 1-D KS tests show us the competing effects which combine in the 2-D case to make it difficult to make a definitive determination between LMC and background source star populations.

6. BEYOND THE ALL OR NOTHING HYPOTHESIS

Thus far we have considered the possibilities that the observed MACHO source stars are either all LMC stars or all background stars at a mean distance of ~ 7 kpc behind the LMC. However, as discussed in Zhao (1999), Zhao (2000) and Zhao, Graff & Guhathakurta (2000) there is substantial middle ground. In a complete analysis, we may treat both the fraction of source stars drawn from the background population and the distance to the background population as adjustable parameters. While the size, location and content of the LMC has been well constrained by observations, the existence, size and location of a background population to the LMC is constrained only by the fact that it must be small enough to have evaded direct detection. The distance to the background population from Zhao, Graff & Guhathakurta (2000) is very loosely derived by the requirement that the background population be at least transiently gravitationally bound to the LMC. However, the reddening of a background population is a much more physically constrained number, a population behind the LMC should certainly suffer from the mean internal extinction of the LMC, a number which has been well determined in a number of studies including Oestricher & Schmidt-Kaler (1996) and Harris, Zaritsky & Thompson (1997). Therefore, all our background population models have the same reddening $\langle E(B-V) \rangle = 0.13$, drawn from the mean extinction of the LMC from Harris, Zaritsky & Thompson (1997) corrected for Galactic foreground extinction.

We define f_{MACHO} to be the fraction of the source stars drawn from the LMC disk population, leaving a fraction $1.0 - f_{MACHO}$ source stars drawn from the background population, and $\Delta\mu$ to be the excess distance modulus of the background population. The term f_{MACHO} is drawn from Zhao, Graff & Guhathakurta (2000) and is meant to emphasize that if a fraction f_{MACHO} of the source stars are LMC stars, then a fraction $\sim f_{MACHO}$ of the microlensing events will be halo lensing events by MACHOs. We consider values $\Delta\mu = 0.0, 0.30, 0.45$ and for each value of the distance modulus we consider the full range of f_{MACHO} from 0.0 to 1.0. For example, a model with $\Delta\mu = 0.45$ and $f_{MACHO} = 0.5$ contains a mixture of source stars in which half the source stars are drawn from the population of the LMC disk, and half the source stars are drawn from a background population displaced from the LMC by ~ 7 kpc and reddened by $\langle E(B-V) \rangle = 0.13$. All models with $f_{MACHO} = 0.0$ contain only source stars drawn from the specified background population, and all models with $f_{MACHO} = 1.0$ are identical, containing only stars drawn from the LMC disk.

We present the results in Figure 8, showing the KS test probabilities as a function of f_{MACHO} for each of our values of $\Delta\mu$. We show the 2-D KS test of the CMD in the bottom panel and the 1-D color and magnitude distribution tests in the middle and top panel, respectively. Again, the error bars reflect the scatter about the mean for one hundred simulations of each model. We note that since all models with $f_{MACHO} = 1.0$ contain only source stars drawn from the LMC disk, all curves for different $\Delta\mu$ must converge at $f_{MACHO} = 1.0$. Furthermore, we learn from Figure 8 that the value of $\Delta\mu$ makes little difference even at $f_{MACHO} = 0.0$. So long as the background population is behind the LMC and therefore reddened by $\langle E(B-V) \rangle = 0.13$ its exact displacement is of little import. In all cases a smaller value of $\Delta\mu$ flattens the curves somewhat. This is expected as a smaller value of $\Delta\mu$ implies overall less difference between the two extreme models at $f_{MACHO} = 0.0$ and $f_{MACHO} = 1.0$.

For all values of $\Delta\mu$ we find that luminosity distributions favor all background source stars ($f_{MACHO} = 0.0$) while the color distributions favor all LMC source stars ($f_{MACHO} = 1.0$). This is in accordance with the analysis of section 5, however there was no reason to expect this result a priori. While we had already constrained the ends of the curve (at least for $\Delta\mu = 0.30$), there may have been local maxima between these two curves. The two dimensional KS test of the CMD displays just such a maximum at $f_{MACHO} \sim 0.4$. This maximum is very shallow on the right hand side and we conclude only that the CMD test favors a value of $f_{MACHO} \gtrsim 0.4$.

7. CONCLUSIONS

We compare two models for the LMC microlensing: source stars drawn from the average population of the LMC and source stars drawn from a population at the far side or behind the LMC. The first model implies that MACHO microlensing is dominated by halo-lensing, while the second implies domination by LMC self-lensing. By comparing the CMD of observed microlensing source stars to a CMD representing all detectable microlensing events for each of these models we find by two-dimensional KS tests that the data suggest that all the source stars are not drawn from the background population. We also compare the one dimensional color and luminosity distributions of observed microlensing source stars with the corresponding model distributions in an effort to understand why our 2-D tests have such little leverage. We find that the 2-D results are governed by two competing factors, an observed luminosity distribution which favors source stars behind the LMC and an observed color distribution which favors source stars in the LMC.

We also consider a number of intermediate models in which we vary the distance modulus of the background population as well as the fraction of stars drawn from average and background populations. In these models we find that for all displacements the most likely model according to our full 2-D CMD analysis occurs for a mixture of 40% LMC stars and 60% background stars. However, the likelihoods decrease only slightly for increasing fraction of LMC stars, and we conclude only that we favor a halo-lensing fraction of $f_{MACHO} \gtrsim 0.4$. For all displacements, models which contain only background stars are the least likely.

At present, the strength of this analysis is severely limited by the number of microlensing events for which we have corresponding HST data. A fortuitous distribution in the CMD of all 13 criterion A events presented in Alcock et al. (2000a) may allow us to definitively exclude an all self-lensing model.

However, a CMD of 20-25 events is necessary to guarantee an answer at the 99% confidence level. Even more events are necessary to exclude mixed models with various fractions of halo and self-lensing. Ongoing microlensing search projects (EROS, OGLE II) should supply a sufficient sample of events in the next few years. The technique outlined in this paper should prove a powerful method for locating the lenses with these future datasets.

Work performed at LLNL is supported by the DOE under contract W7405-ENG-48. DM is also supported by Fondecyt 1990440. CWS thanks the Packard Foundation for the generous support. WJS is supported by a PPARC Advanced Fellowship. CAN is supported in part by a NPSC Graduate Fellowship. TV and KG were supported in part by the DOE under grand DEF0390-ER 40546. TV was supported in part by an IGPP grant.

APPENDIX

REFERENCES

- Alcock, C., et al. 1995, *ApJ*, 454, L125
 Alcock, C., et al. 2000a, *ApJ*, 542, 000
 Alcock, C., et al. 2000b, *ApJ*, in press, astro-ph/0003236
 Alves, D.R. & Nelson, C.A. 2000, *ApJ*, in press, astro-ph/0006018
 Bennett, D.P., et al. 1996, in *Nucl. Phys. B (Proc. Suppl.)*, Vol. 51B, Sources and Detection of Dark Matter in the Universe, ed. D. Cline (Elsevier Science), 131 (astro-ph/960612)
 Evans, N.W. & Kerins, E. 2000, *ApJ*, 529, 917
 Fasano, G., & Franceschini, A. 1987, *MNRAS*, 225, 155
 Geha, M., et al., 1998, *AJ*, 115, 1045
 Gould, A. 1992, *ApJ*, 392, 442
 Gould, A. 1995, *ApJ*, 441, 77
 Gyuk, G., Dalal, N., & Griest, K. 2000 *ApJ*, 535, 90
 Harris, J., Zaritsky, D., & Thompson, I. 1997, *AJ*, 114, 1933
 Holtzman, J.A., et al. 1995, *PASP*, 107, 1065
 Oestricher, M.O., & Schmidt-Kaler, T. 1996, *A&AS*, 117, 303
 Olsen, K.A.G., 1999, *AJ*, 117, 2244
 Olszewski, E.W., Suntzeff, N.B., & Mateo, M. 1996, *ARA&A*, 332, 1
 Peacock, J.A., 1983, *MNRAS*, 202, 615
 Press, W.H., Teukolsky, S.A., Vetterling, W.T., & Flannery, B.P. 1992, *Numerical Recipes in C*, Second Edition (Cambridge: Cambridge Univ. Press)
 Sahu, K.S. 1994 *Nature*, 370, 275
 Schlegel, D.J., Finkbeiner, D.P., & Davis, M. 1998, *ApJ*, 500, 525
 Stetson, P.B. 1987, *PASP*, 99, 191
 Stetson, P.B. 1991, *Data Analysis Workshop III (Garching: ESO)*, 187
 Tomaney, A.B., & Crotts, A.P.S. 1996, *AJ*, 112, 2872
 Weinberg, M. 2000, *ApJ*, 532, 922
 Wu, X. 1994, *ApJ*, 435, 66
 Zhao, H. 1999, *ApJ*, 527, 167
 Zhao, H. 2000, *ApJ*, 530, 299
 Zhao, H., Graff, D.S., & Guhathakurta, P. 2000, *ApJ*, 532, L37

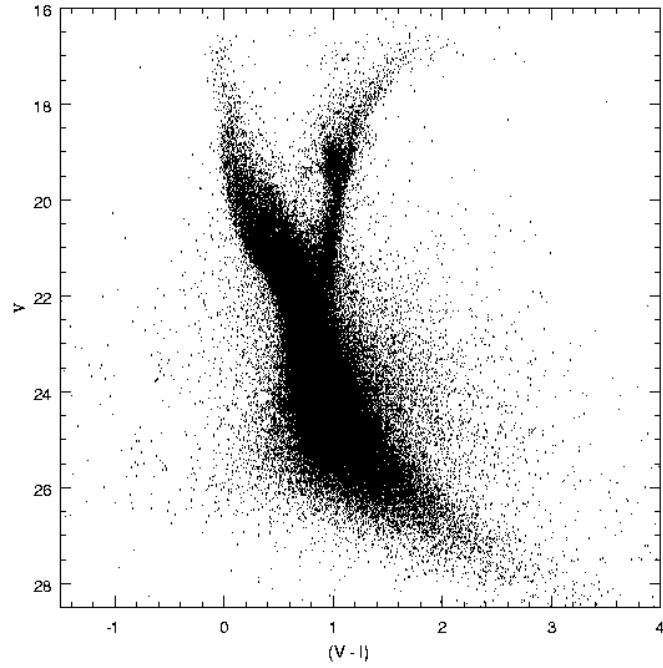


FIG. 1.— The composite HST CMD created by combining the photometry from 8 WFPC2 fields centered on observed MACHO microlensing events.

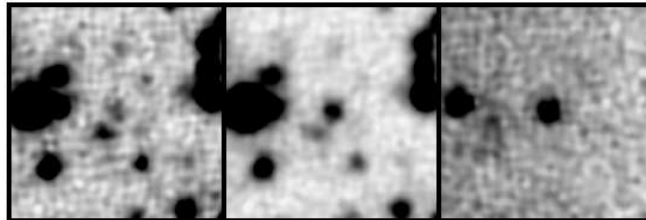


FIG. 2.— The left panel shows a $0.6' \times 0.6'$ section of the baseline image of MACHO event LMC-4. The middle panel shows the same region taken at the peak of the microlensing event. The right panel shows the differenced image. The flux at the left hand side of the differenced image is due to an asymptotic giant branch variable star at that location.

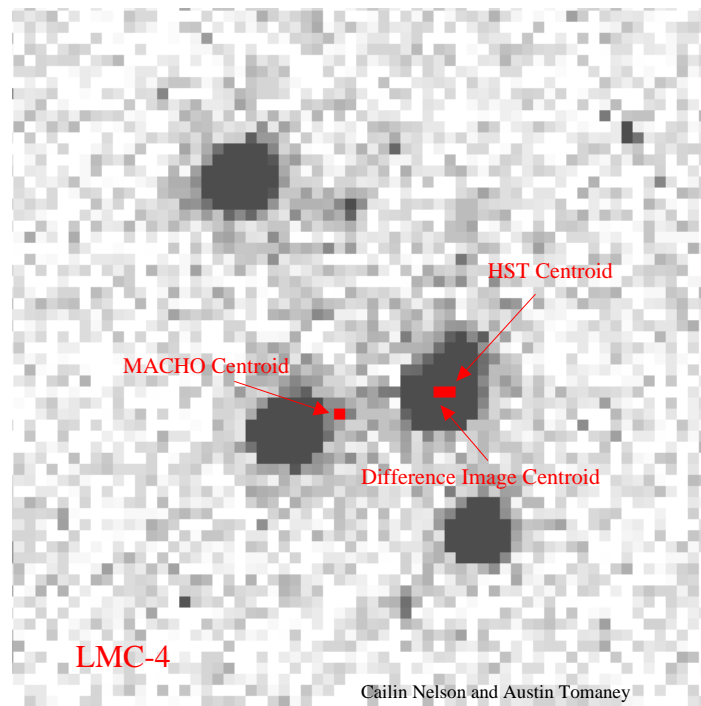


FIG. 3.— A 3'' X 3'' HST image of LMC-4. The circle contains the several HST stars which are all contained within the MACHO seeing disk of the lensed object. The arrows indicate the MACHO baseline centroid, the DIA centroid and the HST centroid.

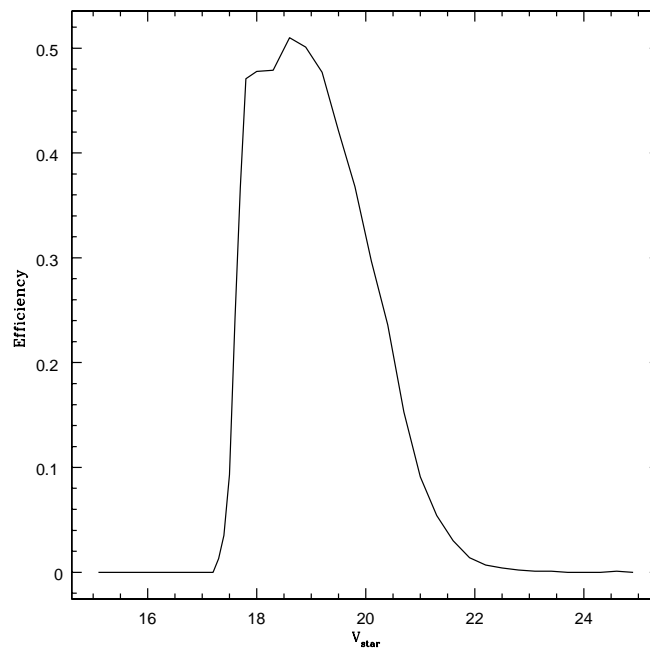


FIG. 4.— The MACHO detection efficiency as a function of stellar V -magnitude. That is, if a microlensing event occurs in a *star* of given magnitude V_{star} , this is the given efficiency for detecting that event.

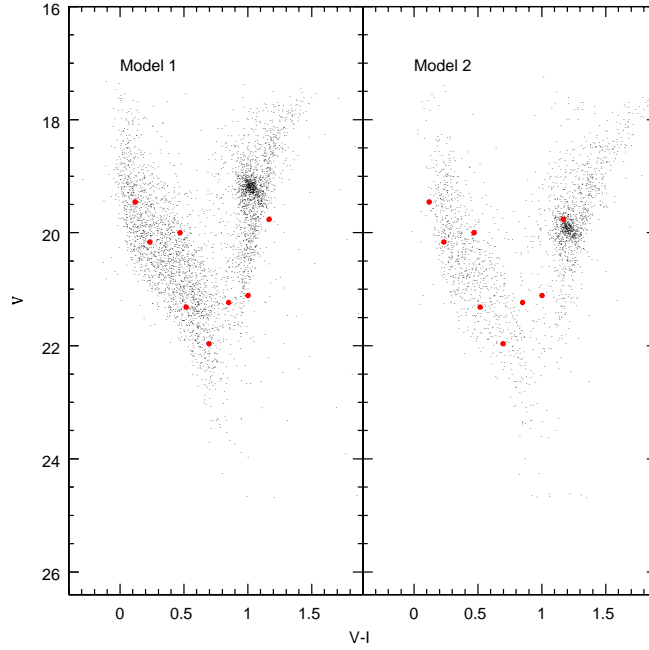


FIG. 5.— The model source star populations. Model 1 represents a source star population in the disk of the LMC, Model 2 represents a source star population behind the LMC. The MACHO microlensing events of Table 2 are overplotted in red. We perform 2-D KS tests to determine whether the microlensing events are drawn from each model source star populations. We find probabilities $P_1 = 0.343 \pm 0.032$ and $P_2 = 0.138 \pm 0.021$ that the microlensing events are consistent with the source star populations of Models 1 and 2, respectively.

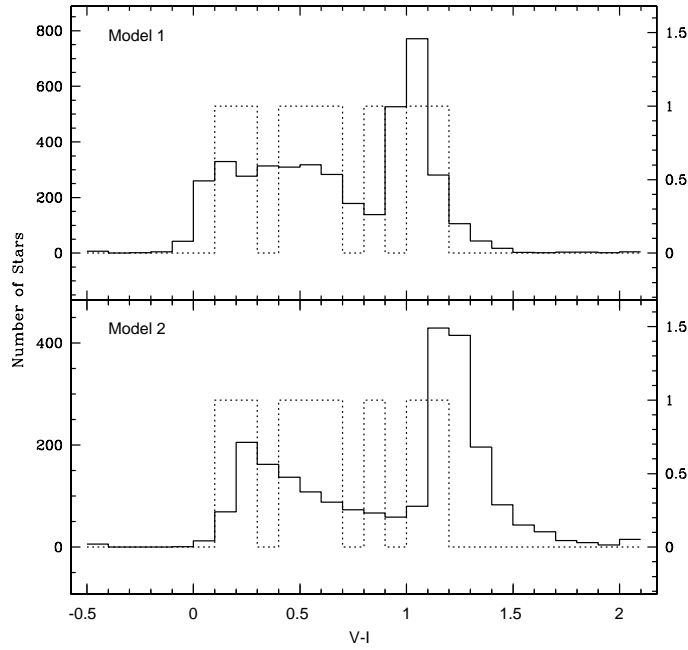


FIG. 6.— The dashed lines show the color function of the observed MACHO microlensing source stars. The solid lines show the color function of the efficiency convolved CMDs for each model. All curves are normalized to have the same total area. We show the actual number of stars in the dashed-line distribution on the right and for the solid-line distribution on the left. We perform 1-D KS tests which return probabilities $P_1 = 0.927$ and $P_2 = 0.065$ that the dashed line distributions are consistent with the solid line distributions.

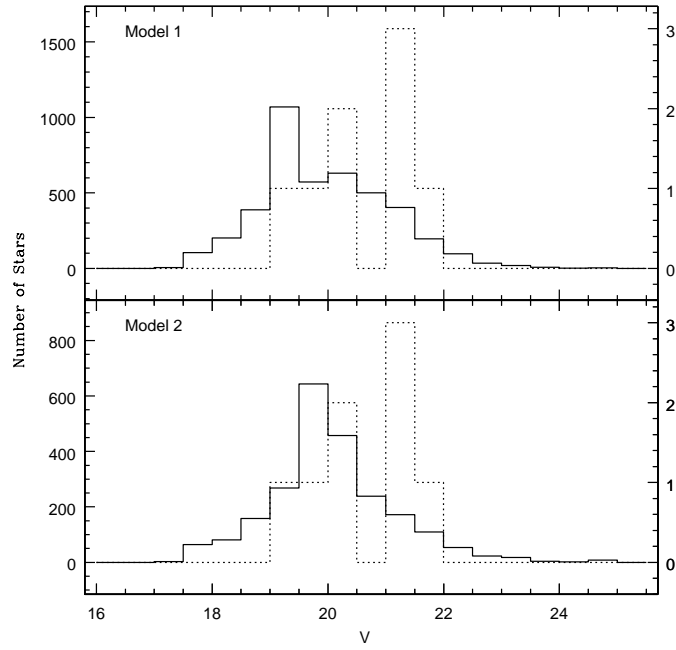


FIG. 7.— The dashed lines show the luminosity function of the observed MACHO microlensing source stars. The solid lines show the luminosity function of the efficiency convolved CMDs for each model. The y-axes are labeled as in Figure 6. We perform 1-D KS test which return probabilities $P_1 = 0.113$ and $P_2 = 0.230$ that the dashed line distributions are consistent with the solid line distributions.

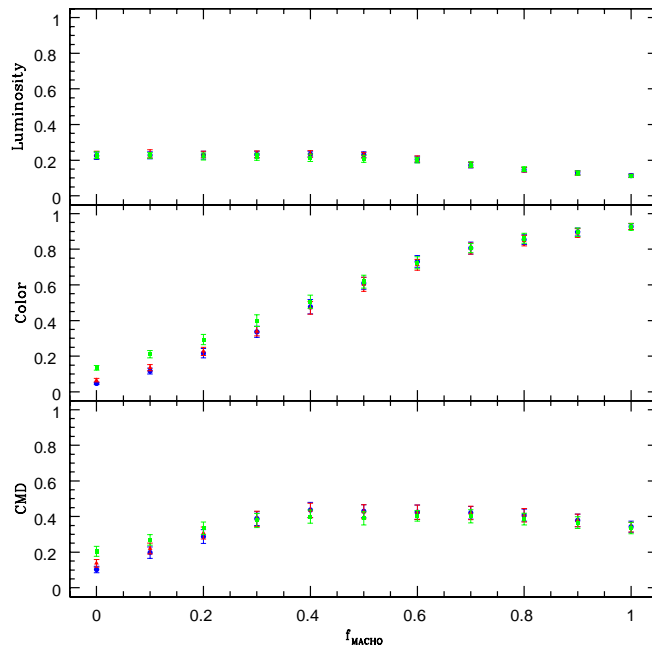


FIG. 8.— The KS test probabilities for various values of f_{MACHO} and $\Delta\mu$ for the 2-D KS test of the CMD test and the 1-D KS test of the luminosity and color distribution tests. We show the results for $\Delta\mu = 0.45, 0.30, 0.0$ in blue circles, red triangles and green squares, respectively. The error bars indicate the scatter around the mean value of hundred simulations done for each model.

TABLE 1
SUMMARY OF OBSERVATIONS

Event	RA	DEC	V Exposure Times	I Exposure Times	Obs Date
LMC-1	05:14:44.50	-68:48:00.00	4X400s	40X500s	1997-12-16
LMC-4	05:17:14.60	-70:46:59.00	4X400s	2X500s	1998-08-19
LMC-5	05:16:41.10	-70:29:18.00	4X400s	2X500s	1999-05-13
LMC-6	05:26:14.00	-70:21:15.00	4X400s	2X500s	1999-08-26
LMC-7	05:04:03.40	-69:33:19.00	4X400s	2X500s	1999-04-12
LMC-8	05:25:09.40	-69:47:54.00	4X400s	2X500s	1999-03-12
LMC-9	05:20:20.30	-69:15:12.00	4X400s	2X500s	1999-04-13
LMC-14	05:34:44.40	-70:25:07.00	4X500s	4X500s	1997-05-13

TABLE 2
PHOTOMETRY OF MICROLENSING SOURCE STARS

Event	V	$V-I$
LMC-1	19.763 ± 0.003	1.167 ± 0.004
LMC-4	21.316 ± 0.008	0.518 ± 0.009
LMC-5	21.233 ± 0.006	0.850 ± 0.012
LMC-6	20.001 ± 0.004	0.470 ± 0.007
LMC-7	21.963 ± 0.013	0.697 ± 0.022
LMC-8	20.164 ± 0.004	0.234 ± 0.009
LMC-9a	21.111 ± 0.007	1.002 ± 0.011
LMC-9b	21.224 ± 0.008	1.012 ± 0.012
LMC-14	19.456 ± 0.002	0.119 ± 0.004